Ceramics International 45 (2019) 4408–4417

Contents lists available at ScienceDirect

Ceramics International

journal homepage: www.elsevier.com/locate/ceramint

Effect of Ta addition on the microstructures and mechanical properties of in situ bi-phase (TiB_2-TiC_xN_y)/(Ni-Ta) cermets

Hong-Yu Yang[a,b], Zheng Wang[a], Shi-Li Shu[b,c,*], Jian-Bang Lu[d]

[a] National Demonstration Center for Experimental Materials Science and Engineering Education, Jiangsu University of Science and Technology, Zhenjiang 212003, China
[b] Key Laboratory of Automobile Materials, Ministry of Education and Department of Materials Science and Engineering, Jilin University, Changchun 130025, China
[c] State Key Laboratory of Luminescence and Applications, Changchun Institute of Optics, Fine Mechanics and Physics, Chinese Academy of Sciences, Changchun 130033, China
[d] Welding Division of Manufacture Engineering Department, Automotive Engineering Corporation, Tianjin 300113, China

ARTICLE INFO

Keywords:
Cermets
Ta content
Mechanical properties

ABSTRACT

In this work, in situ bi-phase (TiB_2-TiC_xN_y)/(Ni-Ta) cermets were fabricated via a combined combustion synthesis and hot-pressing (CSHP) method in a Ni-Ti-BN-B_4C-Ta system. The effects of Ta addition on the reaction process, phase constituents, microstructures and mechanical properties of the (TiB_2-TiC_xN_y)/(Ni-Ta) cermets were studied. Ta is shown to dilute the system and lead to a small number of intermediate phases ($Ni_{20}Ti_3B_6$ and Ni_3Ti) that are retained in the products. Furthermore, the addition of Ta can markedly refine the ceramic particles and decrease the size and quantity of voids. The evaluation of the mechanical properties revealed that an increase in the Ta content resulted in increases in the compression strength (σ_{UCS}) and hardness and that the fracture strain (ε_f) increased first and then decreased. The cermet with the optimal addition of 5 wt % Ta possessed the best mechanical properties without decreasing the value of ε_f (2.9%). The addition of 5 wt% Ta resulted in a compressive strength of 3.37 GPa and the highest hardness of 1909 Hv, which is an increase of ~16% and ~22%, respectively, compared to cermets without added Ta.

1. Introduction

TiC_xN_y is a solid solution of TiC and TiN that possesses high hardness, strength, oxidation resistance and lower friction than the other ceramic particles [1–3]. Therefore, TiC_xN_y has become an important hard material that is widely used as the base material for cermets. TiC_xN_y combined with binders has been successfully used in cutting tools and wear-resistant materials for use in material processing applications [4,5]. TiB_2 is also used as a constituent in cutting tools, wear parts and parts operating under high-temperature conditions [6,7]. Compared with TiC_xN_y, the hardness of TiB_2 is higher [8]. Other studies [9,10] have suggested that TiB_2 is a particularly useful constituent in composite materials and that it increases the strength and fracture toughness of the matrix. Therefore, researchers have considered that using bi-phase TiC_xN_y and TiB_2 ceramics as the reinforced phase would exhibit better performance than adding a single ceramic component [11–14].

Furthermore, the additions of metal binders, such as Ni, Co, Mo and Fe, are useful for enhancing the density and fracture toughness of composites [15–17]. Additionally, low melting metal binders also decrease the ignition temperature due to the formation of a low-melting-point intermetallic or liquid phase through the reverse eutectic reaction [18,19]. Among these binders, Ni processes good wettability with TiC_xN_y and TiB_2 particles [20–22], and Ni is commonly used to achieve high temperature resistance [23,24]. As such, (TiB_2-TiC_xN_y)/Ni cermet has attracted much attention and many researchers have tried to obtain low-cost and high-performance (TiB_2-TiC_xN_y)/Ni cermets using various methods [25,26]. The combined combustion synthesis and hot-pressing (CSHP) method, which is an effective method for the fabrication of in situ composites, has advantages of having a low energy requirement and a one-step forming process [27–29]. Zhan et al. [1,8] successfully prepared (TiB_2-TiC_xN_y)/Ni cermets using the CSHP method and indicated that Ni could offer an easier mass transfer route for the reactants in the Ti-BN-C system.

In recent years, with the development of the exploration industry and the high-speed and high-efficiency cutting industry, the requirement for comprehensive tool material properties has increased. Therefore, further improving the performance of cermets has become

* Corresponding author at: State Key Laboratory of Luminescence and Applications, Changchun Institute of Optics, Fine Mechanics and Physics, Chinese Academy of Sciences, China.
E-mail address: shushili@ciomp.ac.cn (S.-L. Shu).

https://doi.org/10.1016/j.ceramint.2018.11.118
Received 10 October 2018; Received in revised form 10 November 2018; Accepted 15 November 2018
Available online 16 November 2018

Table 1
Characteristics of the raw materials used in the experiments.

Raw materials	Purity (wt%)	Particle size (μm)
Ni	99.5	~58
Ti	99.0	~25
B_4C	99.0	~3.5
BN	99.0	~3
Ta	99.0	~47

Table 2
Composition of the powder compacts.

Sample	Ta contents (wt%)	Ni contents (wt%)	Ti:B_4C:BN (mole ratio)
1	0	30	9:2:2
2	2	28	9:2:2
3	5	25	9:2:2
4	8	22	9:2:2

the research focus of scholars in this field. Qiu et al. [30] reported that elemental Al could reduce the ignition temperature of the Ni-Ti-B_4C-BN system during the combustion synthesis (CS) process and could enhance the mechanical properties of (TiB_2-TiC_xN_y)/Ni cermets. Wang et al. [21] concluded that the addition of W could reduce TiB_2 and TiC_xN_y particle sizes and increase the hardness of the cermets. Consequently, metallic elements with a low melting point and ductility or high a melting point and hardness added into the Ni-Ti-BN-B_4C reaction systems could affect the reaction process, product and mechanical properties of (TiB_2-TiC_xN_y)/Ni cermets.

It is well known that the transition metal Ta possesses excellent ductility, a low coefficient of expansion and a high corrosion resistance, and it is an important high-melting-point strengthening element in nickel-based alloys [31]. Ta has been reported to simultaneously strengthen the matrix and reinforce the phases in nickel-based alloys [31]. In China, Wu et al. [32] found that the addition of Ta can decrease the transformation temperatures and change the microstructure of Ni-Ti alloys. Zhai et al. [33,34] reported that the addition of Ta can decrease

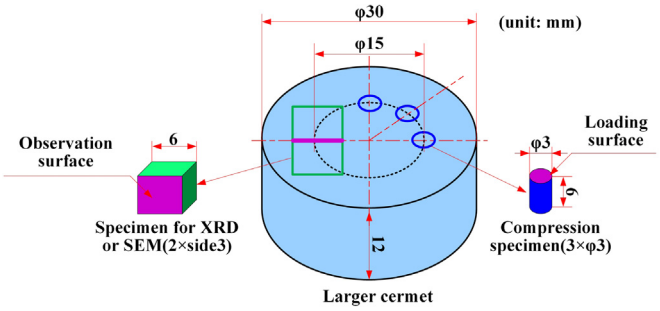

Fig. 2. Sampling diagram for XRD, SEM and the compression test.

the grain size and the amount of precipitate in low activation martensitic steel ingots. However, research into the effect of Ta on the synthesis mechanism, microstructures and mechanical properties of in situ bi-phase ceramic-reinforced cermets is rare. Accordingly, the intensive research performed in the aforementioned works in which Ta was added is meaningful for cermet development.

Hence, in the present work, Ni-Ti-BN-B_4C systems with various Ta contents were used. Then, the in situ bi-phase (TiB_2-TiC_xN_y)/(Ni-Ta) cermets were fabricated via CSHP. The effects of the Ta content on the CS reaction process, phase composition, microstructure and mechanical properties of the (TiB_2-TiC_xN_y)/(Ni-Ta) cermets were studied. The goal of this investigation is to further enhance the performance of (TiB_2-TiC_xN_y)/(Ni-Ta) cermets and to offer guidance for the in situ preparation of bi-phase cermets to improve the construction of materials with high heat resistance and wearability.

2. Experimental

The starting (TiB_2-TiC_xN_y)/(δNi-ωTa) cermet (δ + ω = 30 wt%, and ω = 0, 2, 5 and 8 wt%) materials were made from commercial Ni, Ti, B_4C, BN and Ta powders (Beijing Nonferrous Metals Research Institute, Beijing, China). Detailed information about the starting materials is shown in Table 1. The composition of the compacts for the reaction and

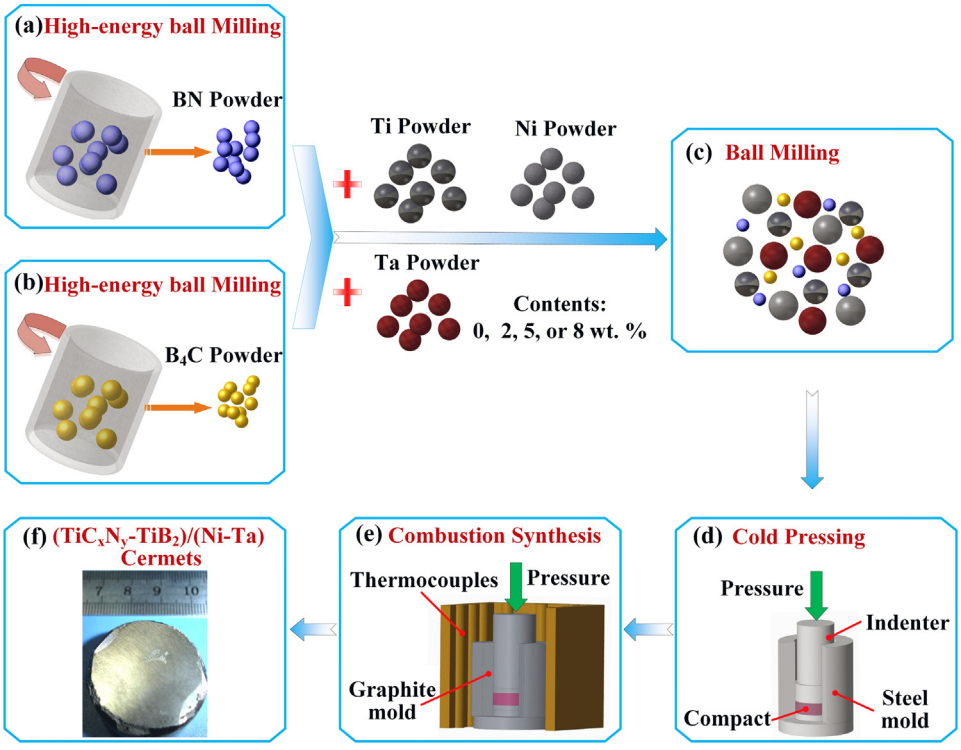

Fig. 1. Schematic diagram of the fabrication process. (a) High-energy ball milling of the B_4C powder; (b) high-energy ball milling of the BN powder; (c) dispersion of the blended powders; (d) blended powders cold pressed into cylindrical compacts; (e) fabrication of (TiB_2-TiC_xN_y)/(Ni-Ta) by CSHP; and (f) the (TiB_2-TiC_xN_y)/(Ni-Ta) cermet samples.

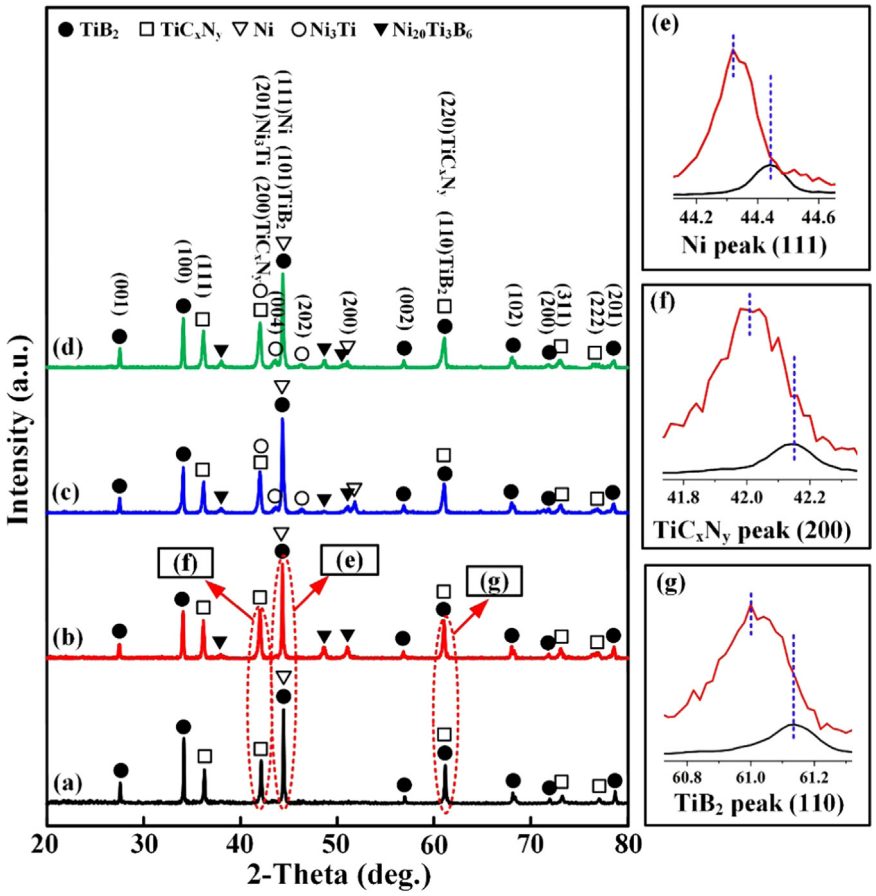

Fig. 3. X-ray diffraction patterns for the (TiB_2-TiC_xN_y)/(Ni-Ta) cermets with different Ta contents: (a) 0, (b) 2, (c) 5, and (d) 8 wt%.

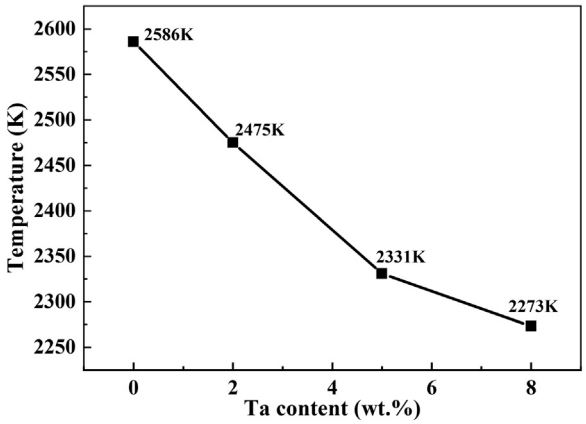

Fig. 4. Variations in the maximum reaction temperature in the Ni-Ti-BN-B_4C system with different Ta contents.

the mole ratio of the starting materials are given in Table 2. The ceramic particle content in the cermets was 70 wt%. The Ti:B_4C:BN molar ratio was 9:2:2, as given in the following equation:

$$9Ti + 2B_4C + 2BN + xNi + yTa \rightarrow 4Ti(C_{0.5}N_{0.5}) + 5TiB_2 + xNi + yTa.$$

The detailed fabrication process is shown in Fig. 1. First, the B_4C and BN powders were activated by high-energy ball milling, as shown in Fig. 1(a) and (b). *A zirconia jar and ZrO_2 grinding ball were used, and the weight ratio of ball to powder was 50:1.* The rating speed was 200 rpm, and the rating time was 2 h. Second, the powders corresponding to 70 wt% (TiB_2-TiC_xN_y)/(Ni-Ta) with 0, 2, 5 and 8 wt% added Ta were blended using a planetary ball mill with ZrO_2 grinding balls (the ball to powder mass ratio was 8). The milling was carried out on a roller ball milling machine at 50 rpm for 24 h, as shown in Fig. 1(c). Third, the mixtures were cold pressed with a pressure of approximately 75 MPa into a cylindrical compact with height of 20 mm and diameter of 30 mm, as shown in Fig. 1(d). Fourth, the powder compact was embedded in a graphite mould in a vacuum furnace. The heating rate of the furnace was ~30 K/min. The reaction temperature of the compact was measured by W/Re thermocouples, and the signals were recorded and processed by a data acquisition system with an acquisition speed of 10 point/s. The sample was quickly pressed at a pressure of 50 MPa for 60 s when the recorded temperature suddenly increased, as shown in Fig. 1(e). Finally, the sample was cooled to room temperature inside the furnace, and the (TiB_2-TiC_xN_y)/Ni cermets *with heights of approximately 12 mm and diameters of 30 mm* were successfully obtained, as shown in Fig. 1(f).

The reactant powders were analysed by differential thermal analysis (DTA, Model TA SDT-Q600, USA) using a heating rate of 40 K/min. The phase composition of the cermets was identified using X-ray diffraction analysis (XRD, Model D/Max 2500PC, Rigaku, Tokyo, Japan). The XRD tests were conducted at a scanning velocity of 4°/min and the scanning range was 20°~80°. Microstructure analyses of the samples were conducted using scanning electron microscopy (SEM, Model Evo18 Carl Zeiss, Oberkochen, Germany) equipped with energy dispersive spectrometry (EDS). All specimens for microstructure observation, constituent analysis and compression tests were taken along the ring at the half radius of the fabricated cermets, as shown in Fig. 2. The TiC_xN_y and TiB_2 particle size measurements were performed using Nano Measurer software.

The cylindrical compression specimens with a diameter of 3 mm and a height of 6 mm were cut from the fabricated cermets by electro-discharge machining, and the loading surface was polished parallel to the

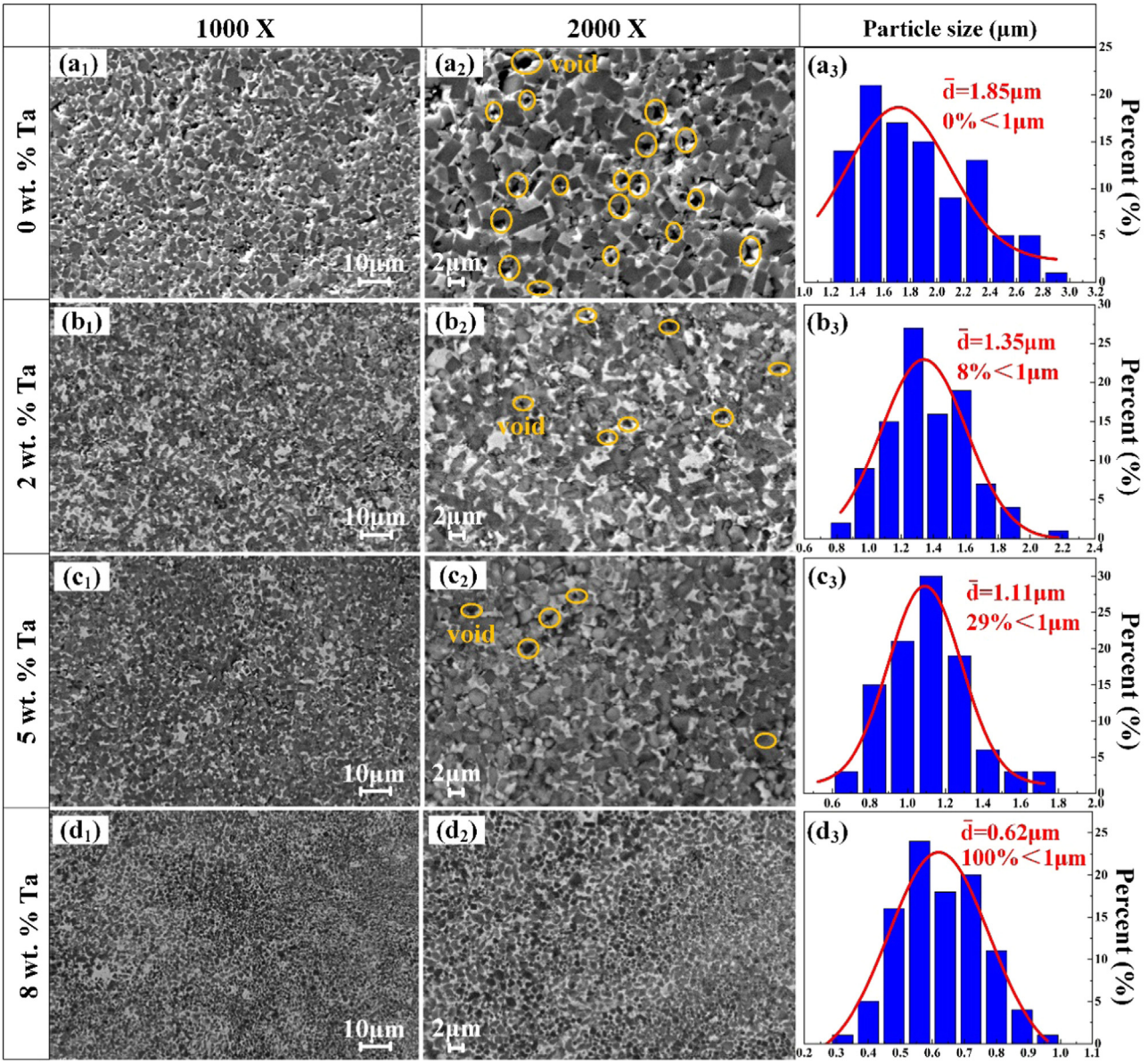

Fig. 5. Microstructures and size distribution of the ceramic particles of the (TiB_2-TiC_xN_y)/(Ni-Ta) cermets with different Ta additions.

other surface. The compression tests were conducted three times for each sample using a servo-hydraulic material testing system (MTS, MTS 810, US) at a strain rate of $1 \times 10^{-4}\ s^{-1}$. The micro-hardness tests were conducted 10 times for each sample on a Vickers hardness tester (Model 1600-5122VD, USA), according to standard ASTM E10–14.

3. Results and discussion

3.1. Ta effect on the phase constituents and microstructures

Fig. 3 shows the XRD patterns of the cermets with 0, 2, 5 and 8 wt% Ta added. As seen in Fig. 3(a), without the Ta addition, only the TiB_2, TiC_xN_y and Ni phases could be detected in the (TiB_2-TiC_xN_y)/Ni cermet. As shown in Fig. 3(b), when 2 wt% Ta was added to the Ni-Ti-BN-B_4C system, a small amount of the $Ni_{20}Ti_3B_6$ phase was detected in the (TiB_2-TiC_xN_y)/(Ni-Ta) cermet. When increasing the Ta content from 2 wt% to 5 or 8 wt%, in addition to $Ni_{20}Ti_3B_6$, some Ni_3Ti was also detected, as shown in Fig. 3(c) and (d). Nonetheless, no metallic Ta or Ta compounds were detected in any samples. However, as shown in Fig. 3(e), with the Ta addition, the peak position of the Ni (111) plane shifted to lower 2θ values, indicating an increase in the interplanar spacing of the Ni (111). By referring to the binary phase diagram of Ni-Ta, it is inferred that the increase in interplanar spacing of Ni was caused by the Ta solid solution in the Ni binder. Since the atomic radius of Ta (0.143 nm) is larger than that of Ni (0.125 nm), the Ta solid solution in Ni leads to a lattice expansion during the process of non-equilibrium solidification. Furthermore, with the addition of Ta, the peak positions of the TiC_xN_y (200) and the TiB_2 (110) planes shift to a lower 2θ. By referring to the binary phase diagram of Ti-Ta, an increase in the interplanar spacing of the TiC_xN_y and the TiB_2 is inferred to be caused by the solid solution of Ta in the Ti lattice, leading to a lattice expansion of the ceramic particles. Based on these results, it is believed that Ta exists in two forms: one form underwent solid solution substitution after diffusing into the binder Ni, and the other form replaced the Ti position in the ceramic particles (TiC_xN_y and TiB_2). In addition, Ta results in the formation of an intermediate phase in the product, and this formation demonstrates the incomplete reaction in the Ni-Ti-BN-B_4C-Ta system with Ta participation. This phenomenon may have two causes. First, the addition of Ta lowers the reaction temperature of the system, as shown in Fig. 4. The maximum combustion temperature of

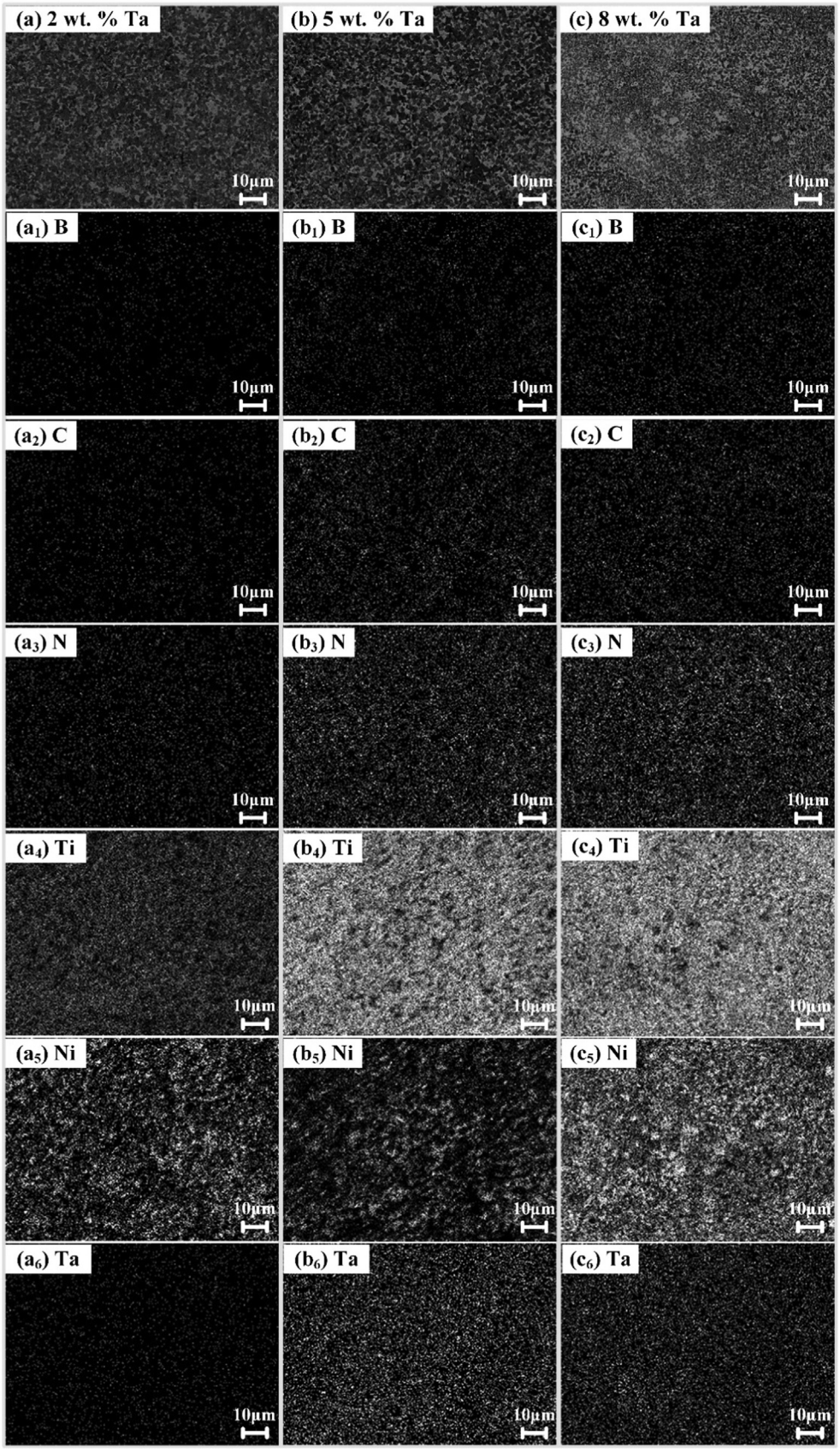

Fig. 6. EDS analysis of the (TiB_2-TiC_xN_y)/(Ni-Ta) cermets with different Ta additions.

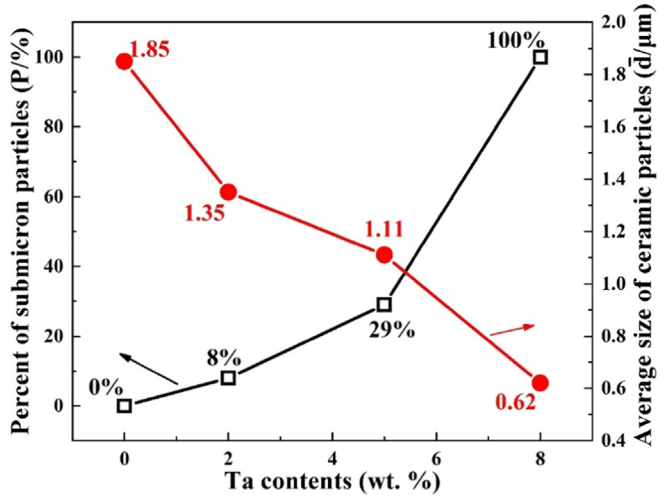

Fig. 7. Variations in the percent of submicron particles and their average size in the ceramic particles of the (TiB_2-TiC_xN_y)/(Ni-Ta) cermets with different Ta additions.

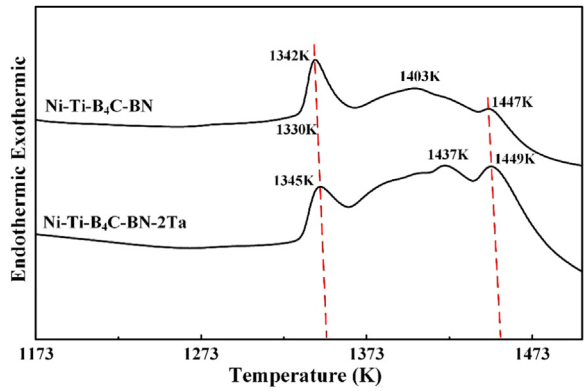

Fig. 8. DTA curves of the Ni-Ti-BN-B_4C system with and without Ta addition.

the system was significantly reduced from 2586 K to 2273 K when the Ta content increased from 0 to 8 wt%. Second, the Ti replacement by Ta results in excess Ti.

Fig. 5 shows the SEM images and size distribution of the ceramic particles for the (TiB_2-TiC_xN_y)/(Ni-Ta) cermets with different Ta additions. As shown in Fig. 5, two types of ceramic particles with different shapes could be distinguished from the microstructures. The TiC_xN_y particles were nearly spherical in shape, and the TiB_2 particles were rectangular in shape. Both the TiC_xN_y and TiB_2 particles have a uniform distribution in the sample. From the EDS analysis of the (TiB_2-TiC_xN_y)/(Ni-Ta) cermets with different Ta contents (Fig. 6), all elements are uniformly distributed without segregation, which again indicates that the Ta exists in both the Ni and ceramic particles. Furthermore, Ta does not cause the aggregation of other elements.

However, when the content of Ta in the samples increases from 0 to 8 wt%, the particle sizes are 1.85, 1.35, 1.11 and 0.62 μm, and the percentages of sub-micron ceramic particles are 0%, 8%, 29% and 100%, respectively. This result means that increasing the Ta content causes the particle size to apparently decrease, and the percentage of sub-micron ceramic particles continuously increases (as shown in Fig. 7). Finally, all ceramic particles are less than one micron in size with the addition of 8 wt% Ta. These results indicate that Ta can significantly refine the particle size, which might be due to the decrease in the reaction temperature. In addition, the size and quantity of voids in these cermets are reduced with an increase in the Ta content (Fig. 5). When the Ta content increases to 8 wt%, the cermets have no appreciable porosity. Ta is expected to improve the wetting between ceramic particles and Ni [35]. Thus, the binder Ni is more likely to fill the smaller voids in the cermets with Ta addition. This result signifies that the interfacial bonding performance between the ceramic particles and Ni is improved with the addition of Ta. According to some reports [36–38], refinement of the reinforcement particles and a decrease in voids are advantageous for enhancing the mechanical properties of composites. To further confirm these results, analyses of the reaction process and the mechanical properties of (TiB_2-TiC_xN_y)/(Ni-Ta) cermets were conducted.

3.2. Ta effect on the reaction mechanism of the Ni-Ti-BN-B_4C system

Fig. 8 shows the DTA results of the Ni-Ti-BN-B_4C with and without Ta addition under a flowing argon atmosphere. In the Ni-Ti-BN-B_4C system, there is a gentle endothermic stage before 1330 K; then, an exothermic peak appears at approximately 1342 K followed by two exothermic peaks at 1403 K and 1447 K. According to some reports [7,8,30,39], a schematic drawing of the reaction is shown in Fig. 9(a), which is an inference of the reaction process. First, before 1323 K, the sluggish solid state diffusion proceeded for Ni, B_4C, Ti and BN, and the Ni_xB_y, TiN_x and TiB phases were primarily developed in this stage. Subsequently, Ni reacted with the resultant TiN_x to form Ni_xTi. Then, Ni-B and Ni-Ti liquids formed between Ni_xB_y and Ni_xTi with a further increase in the temperature. The liquids then diffused to the interspace of the unreacted reactant particles, accelerating the reaction and the facilitating dissolution of B, N and C atoms in the liquids. Second, when the Ni-Ti-B-C-N liquid phase formed, some TiC_xN_y could first be generated during the reaction among [Ti], [C] and [N] ([M] indicates the atoms in this work), causing a remarkable increase in the temperature, consequently igniting the combustion reaction. At this moment, the first intense exothermic peak arises. Third, the increasing temperature further promotes the subsequent dissolution of C, B and N atoms in the Ni-B and Ni-Ti liquids, leading to the formation of Ni-Ti-B-N-C liquid. Subsequently, the TiC_xN_y particles constantly form until the reaction is complete. Furthermore, the formation of TiB_2 commences during the reaction between [Ti] and [B]. At this time, the second moderate exothermic peak arises. Fourth, as the temperature continues to rise, the precipitation of many TiB_2 particles occurs, and the third exothermic peak arises. When the Ti, B, N and C atoms in the liquid are almost exhausted, the reaction finishes.

The reaction process of the Ni-Ti-BN-B_4C system was clearly demonstrated. However, the reaction process after Ta was added to this system has never been investigated. In the Ni-Ti-BN-B_4C-Ta system, these exothermic peaks shift to a higher temperature through the addition of Ta implying that the CS reaction is delayed. A schematic drawing of the reaction when Ta participates is shown in Fig. 9(b). Since there is a total of 30 wt% Ni and Ta in the Ni-Ti-BN-B_4C-Ta system, the Ni content decreases as the Ta content increases. Hence, the addition of Ta can reduce the Ni atom concentration, which indicates that Ta serves as a diluter in the system and delays the CS reaction progress. In addition, the melting point of Ta is approximately 3269 K, and Ta diffuses into the lattice of Ni and Ti during the heating process; thus, Ta continuously absorbs heat from the system during the CS reaction. As a result, the maximum combustion temperature of the system decreases with an increase in the Ta content (as shown in Fig. 4), and this result ultimately leads the incomplete reaction of the Ni-Ti-BN-B_4C-Ta system. Finally, the ceramic particle size is reduced, and a small number of intermediate phases is retained in the product.

3.3. Ta effect on the mechanical properties of the (TiB_2-TiC_xN_y)/(Ni-Ta) cermets

Fig. 10 shows the uniaxial compression curves of the (TiB_2-TiC_xN_y)/(Ni-Ta) cermets with different Ta additions. Clearly, all samples do not exhibit large plasticity. The values of the compression strength (σ_{UCS}), fracture strain (ε_f) and hardness for these cermets are summarized in

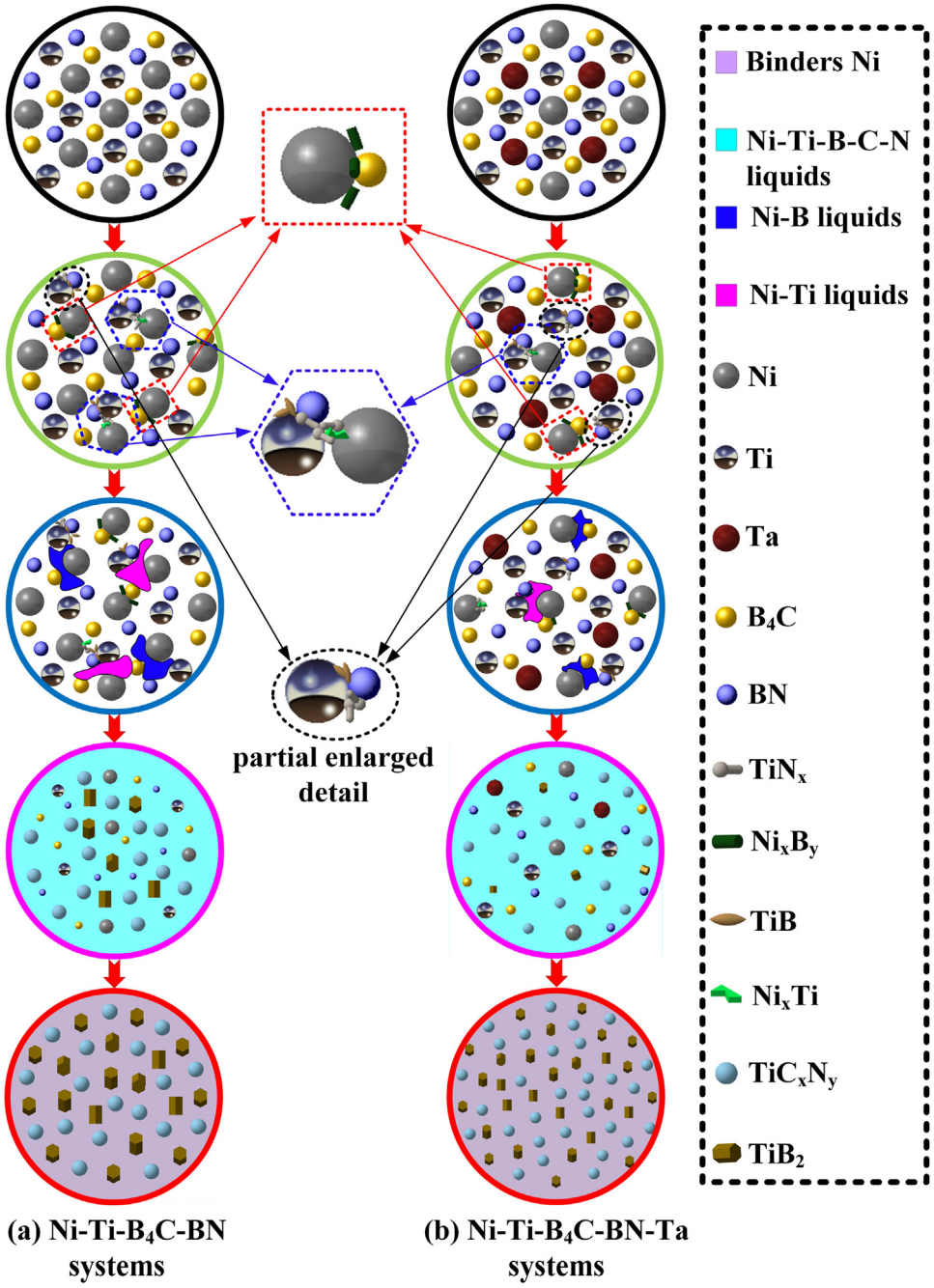

Fig. 9. Schematic diagram of the CS reaction process in the Ni-Ti-BN-B_4C and Ni-Ti-BN-B_4C-Ta systems.

Table 3, and their variations with different Ta contents are shown in Fig. 11. When the Ta content increases from 0 to 8 wt%, σ_{UCS} increases from 2.91 GPa to 3.40 GPa. When the Ta content increases from 0 to 5 wt%, σ_{UCS} shows remarkable strengthening, whereas the improvement of σ_{UCS} is limited when the Ta content increases from 5 wt% to 8 wt%. The mechanical properties of (TiB_2-TiC_xN_y)/(Ni-Ta) cermets depend on the ceramic particles and their interfacial bonding performance [40]. There are three factors contributing to the value of σ_{UCS}. First, a small addition of Ta results in a significant refinement of the TiC_xN_y and TiB_2. Lankford et al. [41] and Staehler et al. [42] demonstrated that the compression strength of composites is highly sensitive to the particle size of the ceramic material. When the cermets have a smaller particle size, the number of particle boundaries per unit volume of the material increases. As a result, the crack-propagation resistance increases. Second, Ta can diffuse into the binder Ni lattice in the form of a substitution solid solution at high temperatures, which causes lattice distortion and increases the strength of the cermets. Third, the addition of Ta can markedly reduce the size and quantity of voids, which improves the interfacial bonding performance between ceramic particles. However, when the Ta content increases to 8 wt%, the degree of incomplete reaction in the Ni-Ti-BN-B_4C-Ta system increases. The increase in the intermediate phases causes a decrease in both the ceramic particles (TiC_xN_y and TiB_2) and the binder Ni to some extent, which is disadvantageous for the strength of the cermets. Therefore, the increasing trend in σ_{UCS} is weakened when the Ta content reaches 8 wt%. As seen from Fig. 11, when the content of Ta increases from 0 wt% to 2 wt%, the ε_f increases from 2.9% to 3.3%. The ε_f improvement may be mainly due to the refinement of the TiC_xN_y and TiB_2 particles with the addition of 2 wt% Ta. Nevertheless, ε_f decreases rapidly to 2.5% when the Ta content increases to 8 wt% because decrease of Ni, the

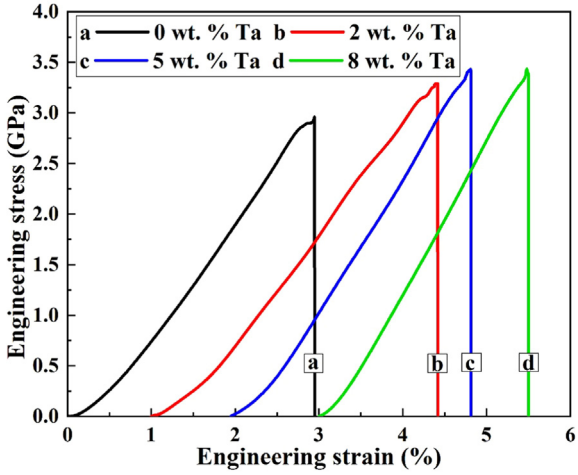

Fig. 10. Compressive engineering stress-strain curves of the (TiB_2-TiC_xN_y)/(Ni-Ta) cermets with different Ta additions: (a) 0, (b) 2, (c) 5, and (d) 8 wt%.

Table 3
Mechanical properties of the (TiB_2-TiC_xN_y)/(Ni-Ta) cermets.

Ta contents (wt %)	Compression strength (σ_{UCS}/GPa)	Fracture strain (ε_f/%)	Hardness (HV)
0	$2.91^{+0.15}_{-0.09}$	$2.90^{+0.20}_{-0.15}$	1561^{+22}_{-44}
2	$3.14^{+0.13}_{-0.11}$	$3.30^{+0.17}_{-0.22}$	1700^{+53}_{-39}
5	$3.37^{+0.16}_{-0.19}$	$2.90^{+0.12}_{-0.16}$	1909^{+86}_{-69}
8	$3.40^{+0.21}_{-0.13}$	$2.50^{+0.11}_{-0.22}$	1879^{+50}_{-79}

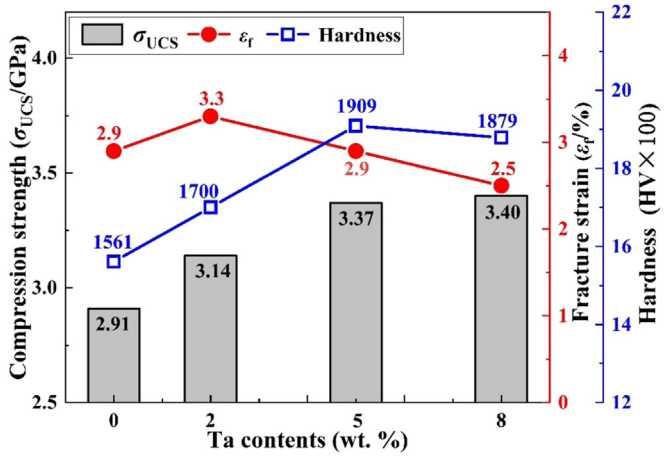

Fig. 11. Variations in the mechanical properties of the (TiB_2-TiC_xN_y)/(Ni-Ta) cermets with different Ta additions.

dissolution of Ta in Ni and the presence of intermediate phases are detrimental to the ε_f of the cermets. As shown in Fig. 11, the hardness of the cermets first increases significantly and then decreases slightly when the Ta content increases from 0 to 8 wt%. The variation in the hardness exhibits a similar trend to that of σ_{UCS}. With the addition of 5 wt% Ta, the cermets exhibit a maximum value of 1909 HV (Table 3). Thus, the (TiB_2-TiC_xN_y)/(Ni-5 wt% Ta) cermet possesses the best mechanical properties without decreasing the value of ε_f (2.9%), and the σ_{UCS} and hardness are 3.37 GPa and 1909 Hv, which are increases of ~16% and ~22%, respectively, compared to the cermet without Ta addition.

Fig. 12 shows the fractured morphologies of the (TiB_2-TiC_xN_y)/Ni cermets containing 0 wt% Ta and 5 wt% Ta. The characteristics of the fracture surface are typically interrelated with the microstructure and mechanical properties of the cermets [43,44]. As shown in Fig. 12(a), for the (TiB_2-TiC_xN_y)/Ni cermet, the fracture morphology presents some intact particles or pits. Furthermore, a propagation of cracks along the interfaces between the ceramic particles and Ni binder occurs on the fracture surface, which means that the connection between the particle boundaries is weak. As shown in Fig. 12(b), for the (TiB_2-TiC_xN_y)/(Ni-Ta) cermet with 5 wt% Ta added, there are no appreciable cracks on the fracture surface, and some crystalline planes are present in the fracture morphology, which means that the propagation of cracks can traverse the Ni binder. This result further confirms that Ta can enhance the interface bonding strength between ceramic particles and the Ni binder.

In general, the cermets are not damaged under pure pressure. However, the microstructure inhomogeneity (such as defects) provides the conditions required for the production of tensile stress, which triggers cracks in the microstructures of the cermets when subjected to a pressure load [45]. A schematic drawing of the crack initiation and propagation is shown in Fig. 13. By comparing the (TiB_2-TiC_xN_y)/Ni cermets with the (TiB_2-TiC_xN_y)/(Ni-Ta) cermets, the size of the ceramic particles is relatively coarse, and the quality and radius of voids are relatively large in the Ta-free cermets. This result means that the microstructure is considerably inhomogeneous. In addition, the presence of fewer particle boundaries leads to hard relaxation of stress at the crack tip. Hence, under the same strain rate, cracks can be nucleated at many locations in the (TiB_2-TiC_xN_y)/Ni cermets. Conversely, for the (TiB_2-TiC_xN_y)/(Ni-Ta) cermets, the size of the ceramic particles is smaller, more particle boundaries are present, and the size and number of voids are reduced. Therefore, the initial crack sources are reduced. Then, after the initiation of a crack, one or more cracks propagate along the weak connections. As discussed above, in the (TiB_2-TiC_xN_y)/Ni cermets, the cracks mainly propagate along the interface between the ceramic particles and Ni (Fig. 13(a)), while in the cermets with Ta addition, the cracks mainly propagate in the binder Ni (Fig. 13(b)).

4. Conclusions

The in situ bi-phase 70 wt% (TiB_2-TiC_xN_y)/(Ni-Ta) cermets with various Ta contents were successfully synthesized using the CSHP method in Ni-Ti-BN-B_4C-Ta systems. The reaction process includes diffusion, dissolution, liquid-state reaction and non-equilibrium solidification. The elemental Ta participated as a diluent during the CS process, which delayed the reaction progress and significantly decreased the maximum combustion temperature. When the Ta content increased from 0 wt% to 8 wt%, σ_{UCS} and the hardness increased, while ε_f first increased and then decreased. The cermet with an optimal Ta content of 5 wt% exhibited the best mechanical properties without decreasing the value of ε_f (2.9%). A compression strength of 3.37 GPa and a hardness of 1909 Hv were obtained, which were increases of ~16% and ~22%, respectively, compared to the cermet without Ta addition. The performance improvement due to the addition of Ta was mainly due to the ceramic particle refinement, the void reduction and the Ta solid solution in the Ni binder and ceramic particles.

CRediT authorship contribution statement

Hong-Yu Yang: Funding acquisition, Conceptualization, Writing - original draft, Formal analysis, Writing - review & editing. **Zheng Wang:** Investigation, Writing - original draft. **Shi-Li Shu:** Funding acquisition, Conceptualization, Formal analysis, Data curation, Writing - review & editing. **Jian-Bang Lu:** Investigation.

Acknowledgments

This work was supported by the National Natural Science Foundation of China (Nos. 51701086 and 51501176).

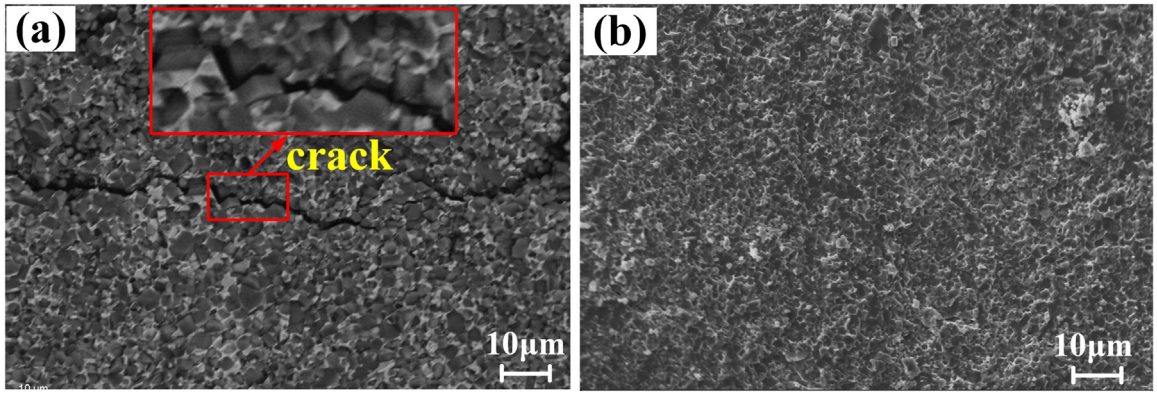

Fig. 12. Fracture surface morphologies of the (a) (TiB_2-TiC_xN_y)/Ni cermets and the (b) (TiB_2-TiC_xN_y)/(Ni-5 wt% Ta) cermets.

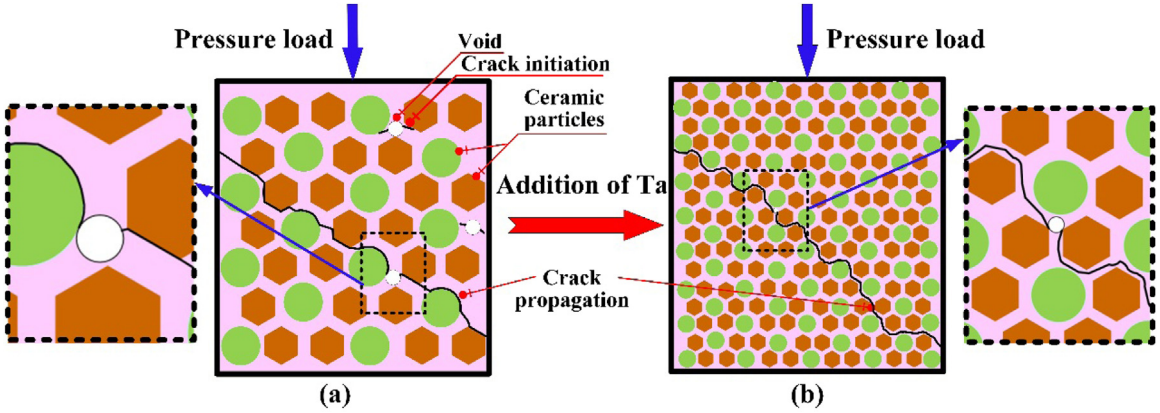

Fig. 13. Schematic drawing of the crack initiation and propagation of the (TiB_2-TiC_xN_y)/(Ni-Ta) cermets (a) without Ta and (b) with Ta additions.

Conflicts of interest

The authors declare that there is no conflict of interest regarding the publication of this paper.

References

[1] L. Zhan, P. Shen, Q.C. Jiang, The mechanism of combustion synthesis of (TiC_xN_y -TiB_2)/Ni from a Ni-Ti-C-BN system, Powder Technol. 205 (2011) 52–60.

[2] W. Yang, J. Xiong, Z.X. Guo, H. Du, T.N. Yang, J. Tang, B. Wen, Structure and properties of PVD TiAlN and TiAlN/CrAlN coated Ti(C, N)-based cermets, Ceram. Int. 43 (2017) 1911–1915.

[3] Z.B. Yin, J.T. Yuan, Z.H. Wang, H.P. Hu, Y. Cheng, X.Q. Hu, Preparation and properties of an Al_2O_3/Ti(C,N) micro-nano-composite ceramic tool material by microwave sintering, Ceram. Int. 42 (2016) 4099–4106.

[4] P. Ettmayer, H. Kolaska, W. Lengauer, K. Dreyert, Ti(C,N) cermets-Metallurgy and properties, Int. J. Refract. Met. Hard Mater. 13 (1995) 343–351.

[5] Q.Z. Xu, J. Zhao, X. Zhao, Fabrication and cutting performance of Ti(C,N)-based cermet tools used for machining of high-strength steels, Ceram. Int. 43 (2017) 6286–6294.

[6] F. Qiu, J.G. Chu, W. Hu, J.B. Lu, X.D. Li, Y. Han, Q.C. Jiang, Study of effect of Zr addition on the microstructures and mechanical properties of (TiC_x-TiB_2)/Cu composites by combustion synthesis and hot press consolidation in the Cu-Ti-B_4C-Zr system, Mater. Res. Bull. 70 (2015) 167–172.

[7] L. Zhan, P. Shen, Q.C. Jiang, The mechanism of combustion synthesis of (TiB2-TiCxNy)/Ni from a Ni-Ti-C-BN system, Powder Technol. 205 (2011) 52–60.

[8] L. Zhan, P. Shen, Q.C. Jiang, Effect of nickel addition on the exothermic reaction of the Ti–C–BN system, Int. J. Refract. Met. Hard Mater. 28 (2010) 324–329.

[9] L.Y. Chen, P. Shen, L.N. Zhang, S. Lu, L.J. Chai, Z.N. Yang, L.C. Zhang, Corrosion behavior of non-equilibrium Zr-Sn-Nb-Fe-Cu-O alloys in high temperature 0.01 M LiOH aqueous solution and degradation of the surface oxide films, Corros. Sci. 136 (2018) 221–230.

[10] V. Marina, B. Alexander, K. Mykola, A.P.A. Marquez, M. Igor, R. Isai, T.R. Guardian,, Formation and properties of TiB_2-Ni composite ceramics, Sci. Sinter. 48 (2016) 137–146.

[11] L.M. Wang, H.L. Liu, C.Z. Huang, B. Zou, X.F. Liu, Effect of sintering process on mechanical properties and microstructure of Ti(C,N)-TiB_2-Ni composites ceramic cutting tool material, Ceram. Int. 40 (2014) 16513–16519.

[12] X. Yue, Z. Cai, X. Lü, J. Wang, H. Ru, Effect of Ni content on microstructures and mechanical properties of hot-pressed TiC-TiB_2-Ni composite, Mater. Sci. Eng. A 668 (2016) 208–214.

[13] A. Moradkhani, H. Baharvandi, M.M.M. Samani, Mechanical properties and microstructure of B_4C-NanoTiB_2-Fe/Ni composites under different sintering temperatures, Mater. Sci. Eng. A 665 (2016) 141–153.

[14] Y.Y. Gao, B.X. Dong, F. Qiu, R. Geng, L. Wang, Q.L. Zhao, Q.C. Jiang, The superior elevated-temperature mechanical properties of Al-Cu-Mg-Si composites reinforced with in situ hybrid-sized TiC_x-TiB_2 particles, Mater. Sci. Eng. A 728 (2018) 157–164.

[15] S.C. Tjong, Z.Y. Ma, Microstructural and mechanical characteristics of in situ metal matrix composites, Mater. Sci. Eng. R. 29 (2000) 49–113.

[16] X.H. Zhang, X.D. He, J.C. Han, W. Qu, V.L. Kvalin, Combustion synthesis and densification of large-scale TiC-xNi cermets, Mater. Lett. 56 (2002) 183–187.

[17] S.L. Shu, C.Z. Tong, F. Qiu, Q.C. Jiang, Effect of Mn, Fe and Co on the compression strength and ductility of in situ nano-sized TiB_2/TiAl composites, SpringerPlus 4 (2015) 784.

[18] Y.F. Yang, D. Mu, Effect of Ni addition on the formation mechanism of Ti_5Si_3 during self-propagation high-temperature synthesis and mechanical property, J. Eur. Ceram. Soc. 34 (2014) 2177–2185.

[19] Y.F. Yang, Q.C. Jiang, Reaction behaviour, microstructure and mechanical properties of TiC-TiB_2/Ni composite fabricated by pressure assisted self-propagating high-temperature synthesis in air and vacuum, Mater. Design 49 (2013) 123–129.

[20] Y.F. Yang, D.K. Mu, Q.C. Jiang, A simple route to fabricate TiC-TiB_2/Ni composite via thermal explosion reaction assisted with external pressure in air, Mater. Chem. Phys. 143 (2014) 480–485.

[21] Y.W. Wang, S.L. Shu, F. Qiu, D.S. Zhou, J.G. Wang, Q.C. Jiang, Effect of W content on the compression properties and abrasive wear behavior of the (TiB_2-TiC_xN_y)/(Ni +W) composites, Mater. Design 45 (2013) 286–291.

[22] S.P. Chen, Q.S. Meng, W. Liu, Z.A. Munir, Titanium diboride-nickel graded materials prepared by field-activated, pressure-assisted synthesis process, J. Mater. Sci. 44 (2009) 1121–1126.

[23] P.J. Zhou, J.J. Yu, X.F. Sun, H.R. Guan, X.M. He, Z.Q. Hu, Influence of Y on stress rupture property of a Ni-based superalloy, Mater. Sci. Eng. A 551 (2012) 236–240.

[24] P.J. Zhou, J.J. Yu, X.F. Sun, H.R. Guan, Z.Q. Hu, Roles of Zr and Y in cast microstructure of M951 nickel-based super alloy, Trans. Nonferr. Met. Soc. 22 (2012) 1594–1598.

[25] E. Shankar, S.B. Prabu, Microstructure and mechanical properties of Ti(C,N) based cermets reinforced with different ceramic particles processed by spark plasma sintering, Ceram. Int. 43 (2017) 10817–10823.

[26] Y.J. Zhao, Y. Zheng, W. Zhou, J.J. Zhang, Q. Huang, W.H. Xiong, Effect of carbon addition on the densification behavior, microstructure evolution and mechanical

properties of Ti(C,N)-based cermets, Ceram. Int. 42 (2016) 5487–5496.
[27] Y.Y. Gao, F. Qiu, S.L. Shu, L. Wang, F. Chang, W. Hu, X. Han, Q. Li, Q.C. Jiang, Mechanical properties and abrasive wear behaviors of in-situ nano-TiC_x/Al-Zn-Mg-Cu composites fabricated by combustion synthesis and hot press consolidation, Arch. Civ. Mech. Eng. 18 (2018) 179–187.
[28] R. Geng, F. Qiu, Q.C. Jiang, Reinforcement in Al matrix composites: a review of strengthening behavior of nano-sized particles, Adv. Eng. Mater. (2018), https://doi.org/10.1002/adem.201701089.
[29] F. Qiu, H.T. Tong, Y.Y. Gao, Q. Zou, B.X. Dong, Q. Li, J.G. Chu, F. Chang, S.L. Shu, Q.C. Jiang, Microstructures and compressive properties of Al matrix composites reinforced with bimodal hybrid in-situ nano-/micro-sized TiC particles, Materials 11 (2018) 1284.
[30] F. Qiu, R. Zuo, S.L. Shu, Y.W. Wang, Q.C. Jiang, Effect of Al addition on the microstructures and compression properties of (TiC_xN_y-TiB_2)/Ni composites fabricated by combustion synthesis and hot press, Powder Technol. 286 (2015) 716–721.
[31] S.M. Cardonne, P. Kumar, C.A. Michaluk, H.D. Schwartz, Tantalum and its alloys, Int. J. Refract. Met. H. 13 (1995) 187–194.
[32] K.H. Wu, J.L. Ma, Effects of Ta addition on microstructure and transformation behavior of Ni-Ti alloys, J. Mater. Sci. Technol. 17 (2001) 5–6.
[33] X.W. Zhai, S.J. Liu, Y.Y. Zhao, Effect of tantalum content on microstructure and tensile properties of CLAM steel, Fusion. Eng. Des. 104 (2016) 21–27.
[34] X.W. Zhai, S.J. Liu, Y.Y. Zhao, K. Wang, Effect of tantalum content on the low cycle fatigue properties of CLAM steel at 823 K, Fusion. Eng. Des. 114 (2017) 211–218.
[35] F. Valenza, S. Gambaro, M.L. Muolo, G. Cacciamani, P. Tatarko, T.G. Saunders, M.J. Reece, A. Schmidt, T. Schubert, T. Weißgärber, A. Passerone, Wetting and interfacial phenomena of Ni-Ta alloys on CVD-SiC, Int. J. Appl. Ceram. Tec. 14 (2017) 295–304.
[36] L. Wang, F. Qiu, Q.L. Zhao, M. Zha, Q.C. Jiang, Superior high creep resistance of in situ nano-sized TiC_x/Al-Cu-Mg composite, Sci. Rep. 7 (2017) 4540.
[37] L. Wang, F. Qiu, S.L. Shu, Q.L. Zhao, Q.C. Jiang, Effects of different carbon sources on the compressive properties of in situ high-volume-fraction TiC_x/2009Al composites, Powder Metall. 59 (2016) 370–375.
[38] F. Qiu, J.G. Chu, W. Hu, J.B. Lu, X.D. Li, Y. Han, Q.C. Jiang, Study of effect of Zr addition on the microstructures and mechanical properties of (TiC_x-TiB_2)/Cu composites by combustion synthesis and hot press consolidation in the Cu-Ti-B_4C-Zr system, Mater. Res. Bull. 70 (2015) 167–172.
[39] L. Zhan, P. Shen, Y.F. Yang, Q.C. Jiang, Self-propagating high-temperature synthesis of TiC_xN_y-TiB ceramics from a Ti-BC-BN system, Int. J. Refract. Met. Hard Mater. 27 (2009) 829–834.
[40] Y.H. Guo, S.W. Liu, Z.Y. Zhang, S.T. Dong, H.Y. Wang, Fabrication of ZnO/Fe rod-like core-shell structure as high-performance microwave absorber, J. Alloy. Compd. 694 (2017) 549–555.
[41] J. Lankford, W.W. Predebon, J.M. Staehler, G. Subhash, B.J. Pletka, C.E. Anderson, The role of plasticity as a limiting factor in the compressive failure of high strength ceramics, Mech. Mater. 29 (1998) 205–218.
[42] J.M. Staehler, W.W. Predebon, B.J. Pletka, G. Subhash, Micromechanisms of deformation in high-purity hot-pressed alumina, Mater. Sci. Eng. A 291 (2000) 37–45.
[43] Y.J. Hwang, S.H. Hong, Y.S. Kim, H.J. Park, Y.B. Jeong, J.T. Kim, K.B. Kim, Influence of silicon content on microstructure and mechanical properties of Ti-Cr-Si alloys, J. Alloy. Compd. 737 (2018) 53–57.
[44] C.D. Rabadia, Y.J. Liu, L. Wang, H. Sun, L.C. Zhang, Laves phase precipitation in Ti-Zr-Fe-Cr alloys with high strength and large plasticity, Mater. Des. 154 (2018) 228–238.
[45] A.V. Dyskin, E. Sahouryeh, R.J. Jewell, H. Joer, K.B. Ustinov, Influence of shape and locations of initial 3-D cracks on their growth in uniaxial compression, Eng. Fract. Mech. 70 (2003) 2115–2136.